

---

# TRANSFERRING THE INHOMOGENEOUS WAVE EQUATION INTO A HOMOGENEOUS EQUATION

---

A PREPRINT

**Marcos V. C. Henriques**

Departamento de Ciências Exatas e Tecnologia da Informação  
Universidade Federal Rural do Semi-Árido  
Angicos, Brazil  
viniciuscandido@ufersa.edu.br

September 30, 2022

## ABSTRACT

The inhomogeneous wave equation, triggered by point sources, forms the basis for the most modern computational techniques of seismic inversion. In this work, we propose to transfer the inhomogeneous wave equation into a homogeneous equation. We show that one can suppress the wavelet-based source term from the inhomogeneous equation in favour of setting the initial time derivative condition of the wavefield as a scaled wavelet of the same type. With the homogeneous wave equation, one can slightly reduce the computational cost of numerical modeling.

**Keywords** wave equation · numerical modelling · wavelets

## 1 Introduction

Many physical phenomena involve the propagation of wavefronts generated by well-localized sources of very short duration. Examples can be found in acoustics [Habets(2006), Allen and Berkley(1979), Ward and Abhayapala(2001)], electromagnetism [Tiwana et al.(2017)Tiwana, Ahmed, Mann, and Naqvi, Vlaar(1966)] and seismology [Vidale and Helmberger(1988), Frankel(1993)]. Modeling such sources is of particular interest in seismic exploration, where the seismic energy is provided in a controlled manner by a high-power short pulse on the surface, triggered by specialized devices such as thumpers or air guns [Evans(1997), Meunier(2011)]. In this case, the wavefronts are responsible for “illuminating” the geological layers interfaces from the subsurface.

The simulation of wave propagation in continuous media, using a numerical solution of the wave equation, is the basis of modern techniques for solving seismic inversion problems. The inversion is a processing stage aimed at directly describing the properties of the rocks. Advanced inversion techniques such as Reverse Time Migration (RTM) [Baysal et al.(1983)Baysal, Kosloff, and Sherwood, McMechan(1989)] and Full Waveform Inversion (FWI) [Virieux and Operto(2009)] massively make use of numerical solutions of the wave equation. The extremely high computational cost of these procedures causes, in most cases, the disregard of elastic effects.

In seismic modeling, an impulsive point source (IPS) is usually represented by a combination of a compact time function, such as a wavelet, and a spatial impulse function, such as the Dirac delta function [Cohen and Bleistein(1979), Alford et al.(1974)Alford, Kelly, and Boore]. The generated wavefronts are characteristic of the chosen wavelet. The wave energy is quickly added to the system as the time wavelet is in action.

Mathematically speaking, setting up sources is not the only way to generate wavefronts. As introduced by d’Alembert in his notorious analytical solution of the homogeneous wave equation [D’Alembert(1747)], initial conditions of the wavefield can trigger the wave propagation. If there are no sources, and therefore no external forces, initial conditions make the system to have, at the initial time, the amount of energy that is going to be propagated. So, depending on the nature of the problem, to model the wave propagation, one could suppress the IPS term in favor of using only the initial conditions. That would be useful, for example, to slightly reduce the computational cost of a simulation.

The intent of this work is to show that, for the one-dimensional case, the waveforms generated by IPS's modeled with time wavelets can be reproduced by setting the initial time derivative of the wavefield as a scaled wavelet of the same type (section 2). This 1D approach can be used as a base for the same methodology in realistic 2D and 3D cases.

## 2 The wave equation

The inhomogeneous wave equation in one dimension can be written as

$$c^2 \partial_x^2 u(x, t) - \partial_t^2 u(x, t) = s(x, t), \quad x \in \mathbb{R}, t \in \mathbb{R}_{\geq 0} \quad (1)$$

where the time-dependent scalar function  $u = u(x, t)$  represents a physical quantity, depending on the problem in which the equation is applied, that produces waves that propagate with velocity  $c$ . For example, it can represent the transverse displacement of a string, the electric or the magnetic field, or seismic waves that travel through the Earth. Accordingly, the source term  $s$ , whose presence characterizes the equation (1) as an inhomogeneous wave equation, can represent an external force applied to a stretched string, point sources of electromagnetic waves such as time-varying charge densities, or a seismic source.

Without the source  $s$ , we have the homogeneous wave equation:

$$c^2 \partial_x^2 u(x, t) - \partial_t^2 u(x, t) = 0, \quad x \in \mathbb{R}, t \in \mathbb{R}_{\geq 0} \quad (2)$$

We will refer to  $u$  as the wavefield. The system of measurement is irrelevant to the discussion of this work, but we choose the International System of Units (SI) for all the fundamental physical quantities. However, the unit of the wavefield  $u$  depends on the nature of the problem. So, throughout the text, we will omit the unit when referring to a value representing the wavefield in a specific position and time.

Let us denote the initial conditions by:

$$\begin{cases} u(x, 0) &= f(x), & x \in \mathbb{R} \\ \partial_t u(x, 0) &= g(x), & x \in \mathbb{R} \end{cases} \quad (3)$$

where  $f$  and  $g$  are smooth functions. The expressions (1) and (3) make up the Cauchy problem for the inhomogeneous wave equation. We will not worry about the boundary conditions, since they do not matter for the main conclusions of this work if the problem domain is infinite, that is, the medium is large enough.

The equation (1) is an example of a hyperbolic partial differential equation, and its solution under conditions (3) is given by [Miersemann(2012)]:

$$\begin{aligned} u(x, t) &= \frac{1}{2} [f(x + ct) + f(x - ct)] + \frac{1}{2c} \int_{x-ct}^{x+ct} g(x') dx' \\ &\quad + \frac{1}{2c} \int_0^t \int_{x-c(t-t')}^{x+c(t-t')} s(x', t') dx' dt' \end{aligned} \quad (4)$$

where the first two terms of the right side make up the d'Alembert solution for the homogeneous wave equation (2), while the third term accounts for the source effects on the wavefield. They are a direct consequence of the *Principle of Causality* [Drábek and Holubová(2014)], which ensures that the value of the solution at a point  $(x, t)$  is only influenced by the values that are within its dependency domain, that is, its *past light cone*. In other words, the effects of a cause cannot influence a point that they did not have time to reach, considering the velocity of propagation  $c$ . So, as one can see in equation (4), if we do not consider sources (third term), the value of  $u(x, t_0 + t)$ , for any  $x$ ,  $t_0$  and  $t$ , depends only on the value of  $u(x - ct, t_0)$  and  $u(x + ct, t_0)$  or on the values of  $\partial_t u|_{t=t_0}$  inside the interval  $x - ct$  to  $x + ct$ .

Let us refer to the three terms of the solution (4) as  $F(x, t)$ ,  $G(x, t)$  and  $S(x, t)$ , respectively:

$$F(x, t) = \frac{1}{2} [f(x + ct) + f(x - ct)], \quad (5)$$

$$G(x, t) = \frac{1}{2c} \int_{x-ct}^{x+ct} g(x') dx', \quad (6)$$

$$S(x, t) = \frac{1}{2c} \int_0^t \int_{x-c(t-t')}^{x+c(t-t')} s(x', t') dx' dt' \quad (7)$$

so that:

$$u(x, t) = F(x, t) + G(x, t) + S(x, t)$$

## 2.1 Impulsive Point source

Especially in seismic exploration, sources are often modeled as impulsive point sources (IPS). Although its time profile is not known in a real survey situation, an IPS  $s(x, t)$  is usually designed by using an integrable and continuous wavelet function  $\psi$  in the following way [Cohen and Bleistein(1979), Alford et al.(1974)Alford, Kelly, and Boore]:

$$s_{x_s, t_s}(x, t) = \psi(t - t_s) \delta(x - x_s) \quad (8)$$

where  $\delta$  is the Dirac delta function,  $t_s$  shifts the wavelet in time and can be interpreted as the instant in which there is the maximum rate of energy release, and  $x_s$  is the location of the source. The use of the Dirac delta function as the spatial part of the model explicits that we are dealing with a point source.

The use of wavelet functions is justified by the fact that they are well localized in both time and frequency, can be easily scaled and translated, and have a zero mean ( $\int_{-\infty}^{\infty} \psi(t) dt = 0$ ) [Mallat(1999)]. Not all wavelets have compact support, but they usually are rapidly decreasing functions and, therefore, vanish at infinity. It is desirable too to use square-integrable functions, that is, satisfying to  $\int_{-\infty}^{\infty} |\psi(t)|^2 dt < \infty$ .

Let us now insert the model (8) into the “source solution” (7) of the wave equation:

$$S_{c, x_s, t_s}^{\psi}(x, t) = \frac{1}{2c} \int_0^t \int_{x-c(t-t')}^{x+c(t-t')} \psi(t' - t_s) \delta(x' - x_s) dx' dt' \quad (9)$$

It can be shown (appendix A), that this integral leads to:

$$S_{c, x_s, t_s}^{\psi}(x, t) = \frac{1}{2c} \left[ \varphi \left( t - t_s - \frac{|x - x_s|}{c} \right) - \varphi(-t_s) \right] \quad (10)$$

where  $\varphi(x)$  is the antiderivative of the wavelet  $\psi(x)$  on every closed interval (in practice, the “indefinite integral” of  $\psi(x)$ ), also having a zero mean. We can interpret  $\varphi$  as the waveform generated by the source. As it will be shown further, the term  $\varphi(t - t_s - |x - x_s|/c)$  takes the form of two wavefronts traveling in the opposite direction to each other.

The solution (10) still reveals that  $t_s$  has to have a positive minimum value that ensures that it is out of the compact subset in which  $\varphi(-t)$  is significative; otherwise, the term  $\varphi(-t_s)$  would add a significant constant to the  $S^{\psi}$  function, causing it not to have zero mean. This guarantees that the brief supplying of energy to the system by the source starts at a time  $t > t_0$ , since the relevant source activity starts before  $t_s$ .

## 2.2 Initial time derivative condition

Consider that the initial time derivative condition  $g(x)$  is given by a wavelet  $\psi(x)$ , scaled and translated as:

$$g_{c, x_s}(x) = \frac{1}{c} \psi \left( \frac{x - x_s}{c} \right) \quad (11)$$

Note that this wavelet is dependent on position  $x$  instead of time  $t$  as in the definition (8) of the source  $s$ . This function is scaled in a different way with which the wavelet is conventionally scaled  $\psi_{c, x_0}(x) = \frac{1}{\sqrt{c}} \psi \left( \frac{x - x_0}{c} \right)$  [Mallat(1999)]. The reason for this choice will become clear later.

With the definition (11), the solution (6) becomes:

$$G_{c, x_s}^{\psi}(x, t) = \frac{1}{2c} \int_{x-ct}^{x+ct} \frac{1}{c} \psi \left( \frac{x' - x_s}{c} \right) dx'$$

It is easy, by substitution of variables, to evaluate this integral and obtain (appendix B)

$$G_{c, x_s}^{\psi}(x, t) = \frac{1}{2c} \left[ \varphi \left( \frac{x - x_s}{c} + t \right) - \varphi \left( \frac{x - x_s}{c} - t \right) \right] \quad (12)$$

in which  $\varphi(x)$  is the antiderivative of the wavelet  $\psi(x)$ . One can note that this solution, as the  $S^{\psi}$ , produces two wavefronts moving in opposite directions to each other. Additionally, the spatial part of this function has mirror symmetry with respect to  $x_s$  position. That is the difference with the  $F$  solution, as defined by (5), which generates waveforms that are simply reduced copies of the initial condition  $f$ : if one sets  $f$  as an asymmetric function, the  $F$  solution will also be asymmetric. This discourages us from using  $f$  to emulate an IPS, since the opposing waveforms produced by a impulsive source have reflection symmetry to each other.

### 2.3 Comparison of waveforms

We are going now to show that the expressions (10) and (12) for  $S$  and  $G$ , respectively, in the special case in which  $\varphi$  is an odd function and vanishes at infinity, generate almost equal waveforms, although out of phase with each other.

**Proposition 1.** *Let  $\varphi$  be an odd function that vanishes at infinity. Let  $G'(\xi, t)$  and  $S'(\xi, t)$  be functions defined by*

$$G'(\xi, t) = \alpha[\varphi(\xi + t) - \varphi(\xi - t)] \quad (13)$$

$$S'(\xi, t) = \alpha[\varphi(t - t_0 - |\xi|) - \varphi(-t_0)] \quad (14)$$

with  $\alpha \in \mathbb{R}_{>0}$ ,  $\xi \in \mathbb{R}$ ,  $t \in \mathbb{R}_{\geq 0}$  and  $t_0 \in \mathbb{R}_{\geq 0}$ . So, for all  $\epsilon \in \mathbb{R}_{>0}$ , there exists a pair  $(\tau, \tau_0) \in \mathbb{R}_{\geq 0}^2$  for which

$$|G'(\xi, t) - S'(\xi, t + t_0)| < \epsilon$$

for all  $\xi \in \mathbb{R}$ ,  $t > \tau$  and  $t_0 > \tau_0$ .

*Proof.* From the  $G'$  and  $S'$  definitions:

$$|G'(\xi, t) - S'(\xi, t + t_0)| = \alpha|\varphi(\xi + t) - \varphi(\xi - t) - \varphi(t - |\xi|) + \varphi(-t_0)| \quad (15)$$

Let us first consider the subset  $\xi \geq 0$ , in which  $\varphi(t - |\xi|) = \varphi(t - \xi)$ . As  $\varphi$  is an odd function,  $\varphi(t - \xi) = -\varphi(\xi - t)$ , and two terms cancel each other on the equation (15):

$$|G'(\xi, t) - S'(\xi, t + t_0)| = \alpha|\varphi(\xi + t) + \varphi(-t_0)| \quad (16)$$

Since  $\varphi$  is a function that vanishes at infinity, given any  $\epsilon > 0$  and  $\alpha > 0$ , one can choose  $\tau$  e  $\tau_0$  such that

$$|\varphi(\xi + \tau)| < \frac{\epsilon}{2\alpha}, \quad |\varphi(-\tau_0)| < \frac{\epsilon}{2\alpha} \quad (17)$$

to any  $\xi \geq 0$ . Therefore, applying to the equation (16) the relations (17) and the subadditivity property of absolute value:

$$|G'(\xi, t) - S'(\xi, t + t_0)| < \epsilon, \quad \forall \xi \in \mathbb{R}_{\geq 0} \quad (18)$$

for all  $t > \tau$  and  $t_0 > \tau_0$ .

For the subset  $\xi < 0$ , in which  $\varphi(t - |\xi|) = \varphi(t + \xi)$ , we get:

$$|G'(\xi, t) - S'(\xi, t + t_0)| = \alpha|-\varphi(\xi - t) + \varphi(-t_0)|$$

Using a procedure similar to that of the case  $\xi \geq 0$ , we achieve the same upper limit as (18):

$$|G'(\xi, t) - S'(\xi, t + t_0)| < \epsilon, \quad \forall \xi \in \mathbb{R}_{<0} \quad (19)$$

Therefore, the proposition is valid in the whole set of real numbers:

$$|G'(\xi, t) - S'(\xi, t + t_0)| < \epsilon, \quad \forall \xi \in \mathbb{R}$$

□

Realize that  $G(x, t)$  and  $S(x, t + t_s)$ , according to the solutions (12) and (10), can be represented in the forms (13) and (14), respectively, with  $\alpha = (2c)^{-1}$ ,  $\xi = (x - x_s)/c$ ,  $c \geq 0$  and  $t_s = t_0$ . Note also that this proposition requires that  $G$  and  $S$  have the same factor  $\alpha$ , what explains our definition (11).

The proposition 1 reveals that, when solving the wave equation (1), if one chooses (11) as the initial condition  $g(x)$  for the time derivative of the wavefield, and sets  $f(x) = 0$  and  $s(x, t) = 0$ , as  $t \rightarrow \infty$ , one gets a solution with waveforms almost identical to those that would be formed if, instead, the function  $s(x, t)$  was defined as an impulsive point source (IPS) modeled as in equation (8). This is the main achievement of this work. It is desirable that  $\varphi(t)$  be a rapidly decreasing function, so that the convergence be fast.

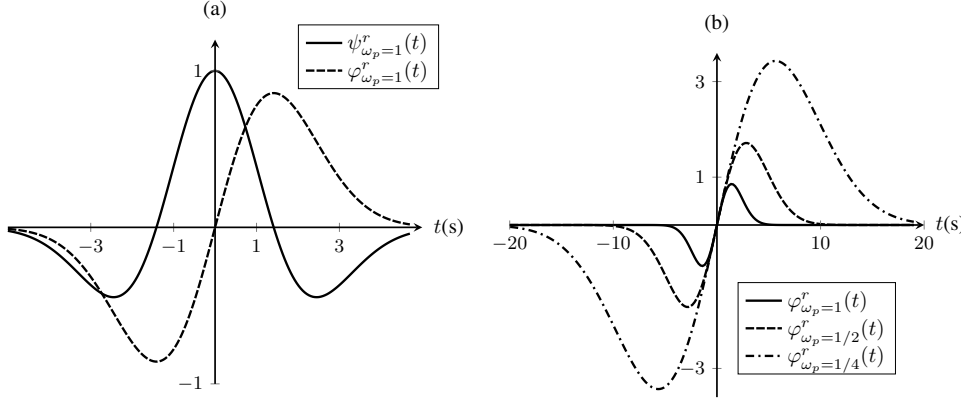


Figure 1: (a) The Ricker wavelet  $\psi^r$ , as defined by (20), with  $\omega_p = 1$  rad/s, and its antiderivative  $\varphi^r$  as defined by (21). (b) Controlling the size of the compact subset in which  $\varphi^r$  is significative.

### 3 Application of the Ricker wavelet

A very commonly used continuous wavelet for modeling short pulses is the Ricker wavelet, which proved to be very suitable for modeling seismic sources [Gholamy and Kreinovich(2014)]. A common definition in time domain is the negative second derivative of a gaussian function[Wang(2015a), Wang(2015b), Wang(2015c)]:

$$\psi_{\omega_p}^r(t) = \left(1 - \frac{\omega_p^2 t^2}{2}\right) e^{-\omega_p^2 t^2/4} \quad (20)$$

where  $t$  is the time in seconds and  $\omega_p$  is the peak frequency, that is, the most energetic frequency, in radians per second. Note that, like other wavelets, this function has zero mean ( $\int_{-\infty}^{\infty} \psi_{\omega_p}^r(t) dt = 0$ ). Its antiderivative function  $\varphi$  corresponds to the first derivative of a gaussian:

$$\varphi_{\omega_p}^r(t) = t e^{-\omega_p^2 t^2/4} \quad (21)$$

As one can see in figure 1-a,  $\psi^r$  is an even function while  $\varphi^r$  is an odd function, that is,  $\psi^r$  is symmetric while  $\varphi^r$  is antisymmetric for any  $\omega_p$ . Even though  $\psi^r$  and  $\varphi^r$  are not compactly supported, they are smooth functions, vanishing at infinity and rapidly decreasing ( $\mathcal{O}(|t|^{-N})$ ,  $\forall N \in \mathbb{R}_{>0}$ ). Therefore,  $\varphi^r$  meets the requirements of proposition 1. By changing the peak frequency  $\omega_p$ , one can manipulate the size of the compact subset in which  $\varphi^r$  and its first derivative  $\psi^r$  are “non-negligible”, as it is shown in figure 1-b. Let us define the extension of the chosen significative subset as

$$\Delta_{n,\omega_p}^{\varphi^r} = n \sigma_{\omega_p} \quad (22)$$

in which  $\sigma_{\omega_p}$  is the standard deviation of the corresponding Gaussian function whose first derivative is  $\varphi_{\omega_p}^r$ , and  $n$  is an integer positive number that sets how many standard deviations are considered. In appendix C it is shown that  $\sigma_{\omega_p} = \sqrt{2}/\omega_p$ . Since the ratio between the value of the zero-centered gaussian function at  $t = 4 \sigma_{\omega_p}$  and its maximum value is of the order of  $10^{-4}$ , we can say that good choices for  $n$  are the ones starting at 4.

The reference frame for the source position is irrelevant, which allow us to set  $x_s = 0$  and omit this parameter from now on. So, the solutions  $S^\psi$  and  $G^\psi$ , as stated by (10) and (12), employing the Ricker wavelet, can be written as

$$S_{c,\omega_p,t_s}^r(x,t) = \frac{1}{2c} \left[ \left( -\frac{|x|}{c} + t - t_s \right) e^{-\omega_p^2(|x|/c - t + t_s)^2/4} + t_s e^{-t_s^2 \omega_p^2/4} \right] \quad (23)$$

$$G_{c,\omega_p}^r(x,t) = \frac{1}{2c^2} \left[ (ct - x) e^{-\omega_p^2(ct-x)^2/4c^2} + (ct + x) e^{-\omega_p^2(ct+x)^2/4c^2} \right] \quad (24)$$

Let us set, for convenience,  $\omega_p = 1$  rad/s and  $c = 1$  m/s. With this choice for  $\omega_p$ , a suitable value for  $t_s$  would be  $\Delta_{4,1}^{\varphi^r}/2 = 4 \sigma_1 = 4\sqrt{2} \text{ s} \simeq 5.66 \text{ s}$ , since we have to guarantee that half of the significant range of the time wavelet fits between  $t = 0$  and  $t = t_s$ . In figures 2-a and 2-b are shown the evolution of (23) and (24), respectively, with uniform

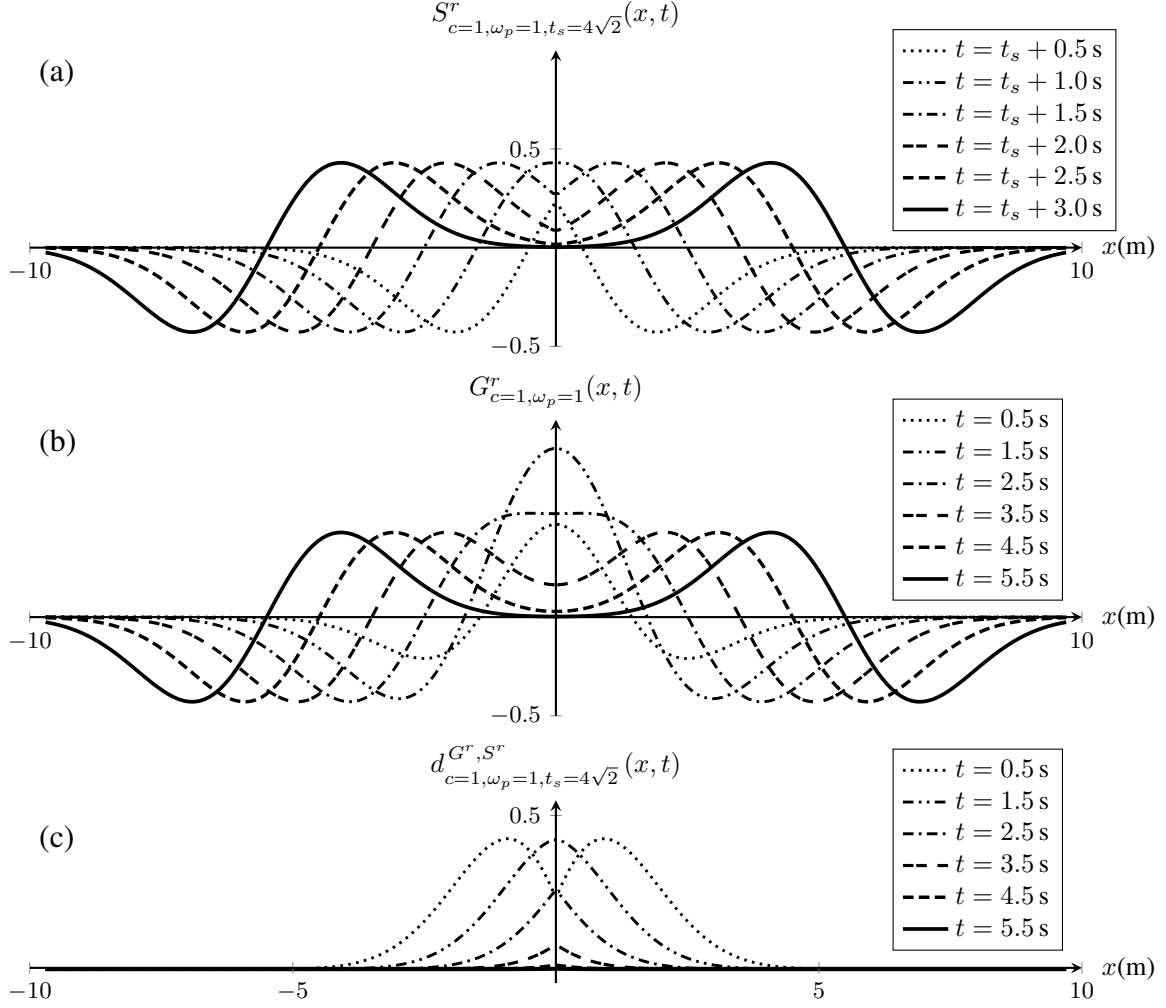


Figure 2: (a) Evolution of  $S^r$  for  $x_s = 0$ ,  $c = 1$  m/s,  $\omega_p = 1$  rad/s and  $t_s = 4\sigma\omega_p = 4\sqrt{2}$  s. (b) Evolution of  $G$  for  $x_s = 0$ ,  $c = 1$  m/s,  $\omega_p = 1$  rad/s. (c) Evolution of the distance operator  $d^{G^r, S^r}_{c=1, \omega_p=1, t_s=4\sqrt{2}}(x, t)$  for  $x_s = 0$ ,  $c = 1$  m/s,  $\omega_p = 1$  rad/s and  $t_s = 4\sigma\omega_p = 4\sqrt{2}$  s.

time intervals. It is remarkable how the two solutions, that start differing from each other, converge quickly to form waveforms of the same shape, amplitude and wavelength. To quantitatively measure this, let us define the following difference operator:

$$d^{G^r, S^r}_{c, \omega_p, t_s}(x, t) = \left| G^r_{c, \omega_p}(x, t) - S^r_{c, \omega_p, t_s}(x, t + t_s) \right| \quad (25)$$

where  $S^r$  is being shifted by  $t_s$ . Figure 2-c presents this comparison, allowing us to see how the difference between the  $G^r$  and  $S^r$  functions decays with the time.

In order to better observe how the difference between  $G^r$  and  $S^r$  depends on  $t$  and is affected by the chosen  $t_s$ , we are now going to define a distance measure operation between  $G^r$  and  $S^r$ . First, let the following norm of an absolutely integrable function dependent on  $x$  and  $t$  be defined:

$$\|f(x, t)\|(t) = \int_{-\infty}^{\infty} |f(x, t)| dx, \quad f \in L^1(\mathbb{R}, x) \quad (26)$$

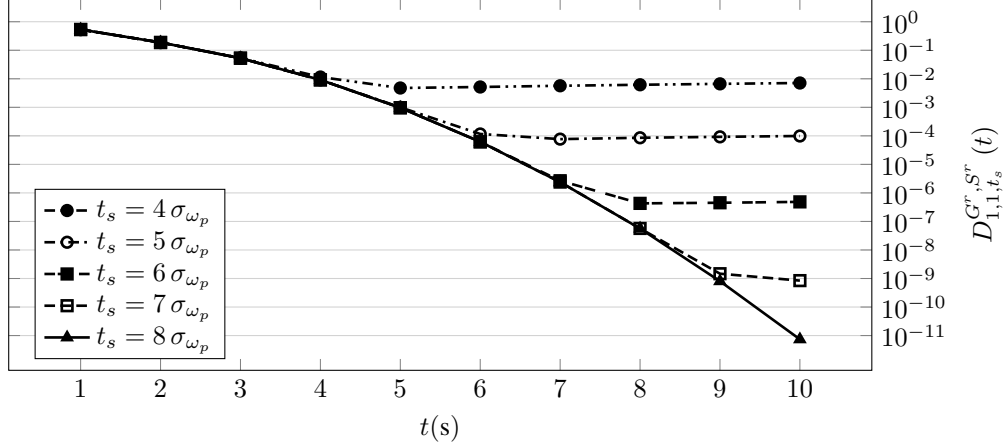


Figure 3: Semi-log plot of  $D_{c, \omega_p, t_s}^{G^r, S^r}(t)$ , as defined by (27), with  $c = 1$  m/s and  $\omega_p = 1$  rad/s, versus  $t$ , to measure how the distance between the  $G^r$  and  $S^r$  solutions decays as the time advances, according to distinct source times  $t_s$ 's.

where  $L^1(\mathbb{R}, x)$  denotes the space of functions that are absolutely integrable in  $x \in \mathbb{R}$  ( $\int_{-\infty}^{\infty} |f(x, t)| dx < \infty$ ). Figure 3 shows the numerical results of calculating the distance operator

$$D_{c, \omega_p, t_s}^{G^r, S^r}(t) = \frac{\|d_{c, \omega_p, t_s}^{G^r, S^r}(x, t)\| (t)}{\|G^r(x, t)\| (t)} \quad (27)$$

where the values of  $t_s$  are in terms of the standard deviation  $\sigma$  of the corresponding gaussian function. The integrals were computed only over the interval from  $x_s - ct - \Delta_{n, \omega_p}^{\varphi^r}/2$  to  $x_s + ct + \Delta_{n, \omega_p}^{\varphi^r}/2$ , since outside it the values of  $G^r$  and  $S^r$  are, by the Causality Principle and the definition of  $\Delta_{n, \omega_p}^{\varphi^r}$ , negligible. The values of  $c$  and  $\omega_p$  were set as 1, with their respective units. As one can see, to the extent that we delay the source time  $t_s$ , the distance between the solutions decays to smaller values as the time advances. However, we have to keep in mind that more delayed  $t_s$ 's result in larger time lags between the  $G$  and  $S$  solutions, what can lead to major discrepancies when dealing with heterogeneous media.

#### 4 Energy analysis of the solutions based on the Ricker wavelet

To a better understanding of how the solutions  $G^{\psi}$  and  $S^{\psi}$  form the wavefield, it is convenient to make an energy analysis of the both solutions. The wave energy can be simply defined as follows:

$$E_c(t) = \frac{1}{2} \int_{-\infty}^{\infty} (\partial_t u)^2 dx + \frac{c^2}{2} \int_{-\infty}^{\infty} (\partial_x u)^2 dx \quad (28)$$

Physically,  $E_c(t)$  is the total energy of the system. The term with  $(\partial_t u)^2$  corresponds to the kinetic energy, while the one with  $(\partial_x u)^2$  corresponds to the potential energy.

$$K(t) = \frac{1}{2} \int_{-\infty}^{\infty} (\partial_t u)^2 dx \quad (29)$$

$$U_c(t) = \frac{c^2}{2} \int_{-\infty}^{\infty} (\partial_x u)^2 dx \quad (30)$$

The homogeneous wave equation (2) has no terms that insert or dissipate energy. Therefore, it is to be expected that the identity  $\frac{d}{dt} E_c(t) = 0$  be valid.

To get the energy expressions associated with the Ricker-based initial derivative solution, one can just substitute  $u$  in (29) and (30) by  $G^r$  (24). The algebraic calculation is straightforward and lengthy, and can be directly done with the

aid of a computer algebra system. The obtained kinetic energy expression is

$$K_{c,\omega_p}^{G^r}(t) = \frac{1}{8c\omega_p} \sqrt{\frac{\pi}{2}} e^{-\frac{1}{2}\omega_p^2 t^2} \left( \omega_p^4 t^4 - 6\omega_p^2 t^2 + 3 + 3e^{\frac{1}{2}\omega_p^2 t^2} \right) \quad (31)$$

and the potential energy

$$U_{c,\omega_p}^{G^r}(t) = \frac{1}{8c\omega_p} \sqrt{\frac{\pi}{2}} e^{-\frac{1}{2}\omega_p^2 t^2} \left( -\omega_p^4 t^4 + 6\omega_p^2 t^2 - 3 + 3e^{\frac{1}{2}\omega_p^2 t^2} \right) \quad (32)$$

One can easily check that both the expressions given in (31) and (32) tend to the same constant value as time tends to infinity. The constant total energy associated with the  $G^r$  solution is the sum of the kinetic (31) and potential (32) energies:

$$E_{c,\omega_p}^{G^r} = \frac{3}{4c\omega_p} \sqrt{\frac{\pi}{2}} \quad (33)$$

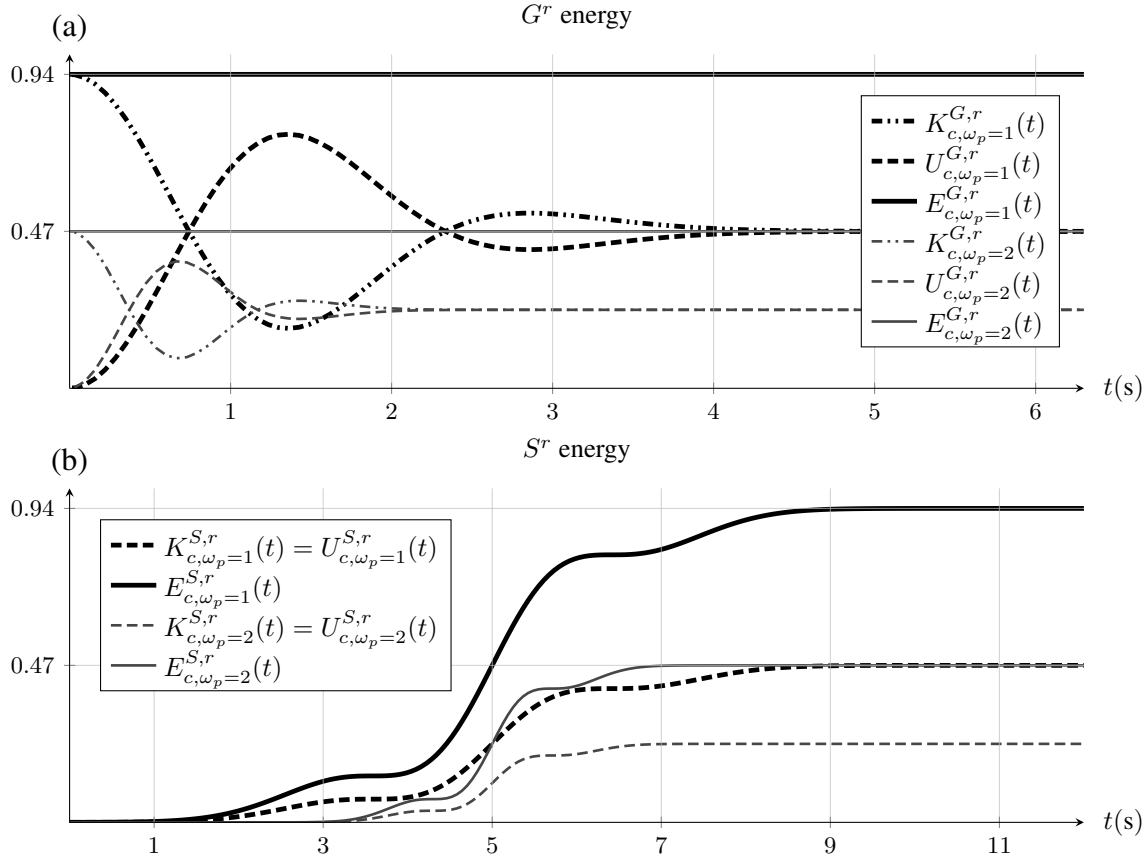


Figure 4: Evolution in time of the kinetic energy  $K_{c,\omega_p}$ , potential energy  $U_{c,\omega_p}$  and total energy  $E_{c,\omega_p}$  for the  $G^r$  and  $S^r$  solutions of the wave equation. There are shown the cases in which the peak frequency  $\omega_p$  is set as 1 rad/s and 2 rad/s. (a)  $G^r$  energy for  $c = 1$  m/s. (b)  $S^r$  energy for  $c = 1$  m/s and  $t_s = 5$  s.

By applying the  $S^r$  solution of the inhomogeneous wave equation (23) to the energy formula (28), and after some tedious calculation, one can get the expression for the kinetic energy:

$$K_{c,\omega_p}^{S^r}(t) = \frac{3}{16c\omega_p} \sqrt{\frac{\pi}{2}} \left[ \operatorname{erf} \left( \frac{\omega_p(t-t_s)}{\sqrt{2}} \right) + 1 \right] - \frac{1}{16c} (t-t_s) e^{-\frac{1}{2}\omega_p^2(t-t_s)^2} \left[ \omega_p^2(t-t_s)^2 - 1 \right] \quad (34)$$

where  $\operatorname{erf}$  is the error function. Curiously, we get the same expression for the potential energy  $U_{c,\omega_p}^{S^r}(t)$ . This equipartition of energy in wave motion is predicted by Duffin[Duffin(1970)], that has shown that, if the solution has



compact support, in an odd-dimensional space, after a finite time, the kinetic energy of the wave is constant and equals the potential energy. Therefore, the total energy has the expression:

$$E_{c,\omega_p}^{Sr}(t) = 2K_{c,\omega_p}^{Sr}(t) = \frac{3}{8c\omega_p} \sqrt{\frac{\pi}{2}} \left[ \operatorname{erf}\left(\frac{\omega_p(t-t_s)}{\sqrt{2}}\right) + 1 \right] - \frac{1}{8c} (t-t_s) e^{-\frac{1}{2}\omega_p^2(t-t_s)^2} \left[ \omega_p^2(t-t_s)^2 - 1 \right] \quad (35)$$

Note that, since the point source inserts energy into the system, the total energy associated with  $S$  varies with  $t$ . However, because of the short duration of the source, it can be easily shown that the maximum value of (35), corresponding to its limit as  $t$  tends to infinity, matches the same  $G^r$  total energy (33) (appendix D):

$$E_{c,\omega_p,\max}^{Sr} = \lim_{t \rightarrow \infty} E_{c,\omega_p}^{Sr}(t) = \frac{3}{4c\omega_p} \sqrt{\frac{\pi}{2}} = E_{c,\omega_p}^{Gr} \quad (36)$$

For example, for the case  $c = 1$  m/s and  $\omega_p = 1$  rad/s, we have  $E_{c,\omega_p,\max}^{Sr} = E_{c,\omega_p}^{Gr} \simeq 0.94$ . In figure 4 is shown the energy evolution of each solution, with two different peak frequencies. In figure 4-a, we can see that all the energy of wave propagation for  $G$  solution is available from the initial time in the form of kinetic energy. We can also observe that, after oscillating during a brief time,  $K^{G,r}$  and  $U^{G,r}$  converge to the same value corresponding to the half of the total energy. As shown in figure 4-b, the IPS releases energy to the system during a time determined by  $\omega_p$  and with a rate that reaches its maximum at  $t_s = 5$  s, and with  $K^{G,r}$  being equal to  $U^{G,r}$  all the time. The effect of setting the peak frequency  $\omega_p$  as 2 rad/s instead of 1 rad/s is to cut the total energy in half, as can be predicted by the equation (36).

## 5 Numerical Implementation

A conventional way of discretizing the inhomogeneous wave equation (1) consists of approximating the derivatives of second order with centered differences in a mesh of grid points  $(x_i, t_n) = (i\Delta x, n\Delta t)$  [Kukudzhanov(2013)]:

$$\begin{cases} \partial_x^2 u(x_i, t_n) \approx \frac{u_{i+1,n} - 2u_{i,n} + u_{i-1,n}}{(\Delta x)^2} \\ \partial_t^2 u(x_i, t_n) \approx \frac{u_{i,n+1} - 2u_{i,n} + u_{i,n-1}}{(\Delta t)^2} \end{cases} \quad (37)$$

where  $i = 1..N_x$  and  $n = 1..N_t$  are the spatial and temporal indexes, respectively. When (37) is applied to the inhomogeneous wave equation (1) leads to the finite difference (FD) scheme

$$u_{i,n+1}^{(s)} = -u_{i,n-1}^{(s)} + 2u_{i,n}^{(s)} + C^2 \left( u_{i+1,n}^{(s)} - 2u_{i,n}^{(s)} + u_{i-1,n}^{(s)} \right) - \Delta t^2 s_{i,n} \quad (38)$$

where the superscript  $(s)$  makes explicit that the energy of this solution is provided by the source, and  $C = c \frac{\Delta t}{\Delta x}$  is the so-called *Courant number*, a dimensionless number that is related to the numerical stability of solving the wave equation by using the finite difference method. We consider the simple case in which  $c$  (and consequently also  $C$ ) is uniform in all the mesh, that is, the medium is homogeneous (not to be confused with the homogeneous wave equation). The Courant–Friedrichs–Lewy (CFL) condition demands that, for one-dimensional case [Courant et al.(1967)Courant, Friedrichs, and Lewy],

$$C \leq 1 \quad (39)$$

The expression (38) provides an iterative procedure for solving the wave equation. Since the time-related index  $n$  is iterated, (38) represents a time-domain FD method.

An Impulsive Point Source (IPS) can be approximated in the discrete domain in the following way:

$$s_{i,n} = \psi_n \delta_{i,i_s} \quad (40)$$

in which  $\psi_n$  is the discrete sampling, at time index  $n$ , of the continuous wavelet  $\psi$  centered at the time  $t_s$ , and  $\delta_{i,i_s}$  represents the Kronecker delta, which is equal to 1 only when  $i = i_s$ , which  $i_s$  being the spatial index that localizes the source.

The time derivative in the initial conditions (3) can be embedded in a simple way by taking the following approximation:

$$\partial_t u(x_i, t_n)|_{n=0} = g_i \approx \frac{u_{i,1} - u_{i,-1}}{2\Delta t} \quad (41)$$

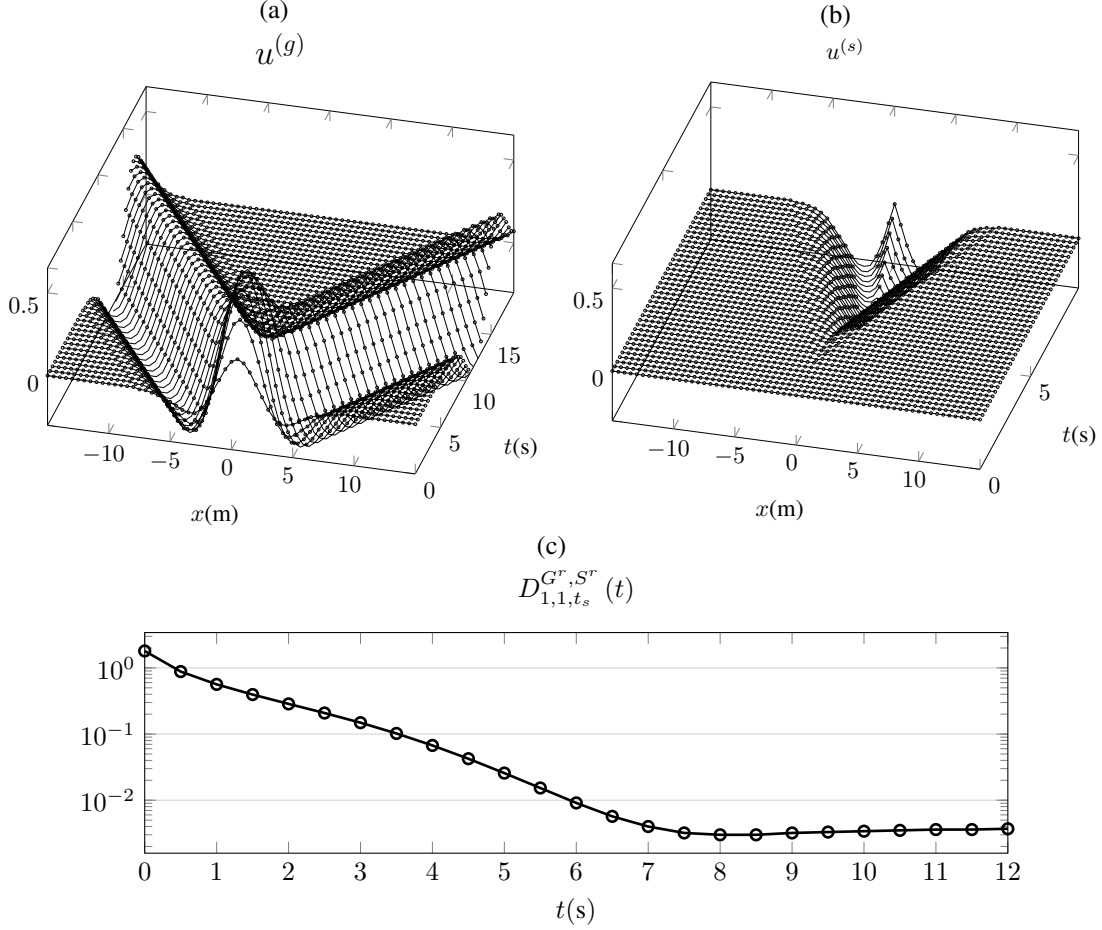


Figure 5: Numerical simulation of wave propagation by solving the wave equation with the finite difference method. (a) Setting the initial time derivative condition, without a source. (b) Setting an impulsive point source (IPS). The parameters are:  $x_s = 0$ ,  $t_s = 10$  s,  $c = 1$  m/s,  $\omega_p = 1$  rad/s,  $\Delta x = 0.5$  m,  $\Delta t = 0.5$  s.

Inserting (41) into (38), with  $n = 0$ , and setting  $s_{i,0} = 0$  at every point of the grid (that is, there is no source acting at the initial time), one gets

$$u_{i,1} = u_{i,0} + \Delta t g_i + \frac{1}{2} C^2 (u_{i+1,0} - 2u_{i,0} + u_{i-1,0}) \quad (42)$$

which corresponds to the first iteration of time-domain FD scheme. If we consider  $u_i^0 = 0$  at every point of the grid (that is, no initial wavefield), the expression is reduced to:

$$u_{i,1}^{(g)} = \Delta t g_i \quad (43)$$

where the superscript  $(g)$  makes explicit that the energy is available from the beginning of the simulation via the time derivative initial condition. Seeing that the computational domain is limited, one has to design artificial boundaries satisfying the chosen boundary conditions. We will not discuss here the artificial boundaries methods, since they are irrelevant to the main point of this work if the spatial domain is large enough.

The present work states that one can substitute a wavelet-based IPS  $s_{i,n}$  by setting  $g_i$  in (42) as the sampled wavelet:

$$g_i = \frac{1}{c} \psi_{(i-i_s)/c} \quad (44)$$

and removing the  $s$  term in (38)

$$u_{i,n+1}^{(g)} = -u_{i,n-1}^{(g)} + 2u_{i,n}^{(g)} + C^2 (u_{i+1,n}^{(g)} - 2u_{i,n}^{(g)} + u_{i-1,n}^{(g)}) \quad (45)$$

Figure 5 presents the results of two simulations by using the described methodologies based on  $s$  and  $g$ , with  $c = 1$  m/s and  $\omega_p = 1$  rad/s. Although the space-time domain is larger, the plot shows a set of points corresponding to  $N_x = 61$  discrete positions, varying from  $x = -15$  m to  $x = 15$  m ( $\Delta x = 0.5$  m), and  $N_t = 41$  discrete times, varying from  $t_0 = 0$  s to  $t = 20$  s ( $\Delta t = 0.5$  s). With this set of parameters, the Courant Number  $C$  equals 1, satisfying the CFL condition (39) in the limit. Figure 5-a shows the evolution of the wavefield when one sets  $g_i$  in the first iteration (43) as the sampled wavelet (44), and use (45) as the FD scheme. Figure 5-b shows the evolution of the wavefield when both  $u_{i,0}$  and  $u_{i,1}$  equal 0 at every point of the grid, and one uses (38) as the FD scheme, with  $s_i$  being defined by (40). The source is located at  $x_s = 0$  and reaches its maximum energy transfer at  $t_s = 10$  s.

To compare these two results, we implement a discrete version of the distance operator (27):

$$D_n^{G,S} = \frac{\sum_{i=1}^{N_x} |u_{i,n}^{(g)} - u_{i,n+n_s}^{(s)}|}{\sum_{i=1}^{N_x} |u_{i,n}^{(g)}|} \quad (46)$$

where  $n_s$  is the time index associated with  $t_s$ . Since  $t_s = 10$  s and  $\Delta t = 0.5$  s, we have for this case  $n_s = 20$ . Figure 5-c shows the evolution of  $D_n^{G,S}$ , demonstrating that the waveform  $u^{(g)}$  comes to have approximately the same shape of  $u^{(s)}$  after about 8 seconds, despite being out of phase, as indicated by the distance measure below  $10^{-2}$  ( $< 1\%$ ). This is not so persuasive as the theoretical prediction expressed in the figure 3, what we credit to the imperfections of the discretizations (37) and (41), but it is still a good clue that the IPS can be numerically emulated by setting a suitable initial time derivative condition, and so slightly reducing the computational cost of the modelling process.

## 6 Conclusions

In time-domain modeling of the wave equation for seismic applications, the wave propagation is usually triggered by setting a wavelet-based source term. We have shown that, by using a scaled wavelet as the initial time derivative condition of the one-dimensional homogeneous wave equation, one can generate the same waveforms that would be generated by an impulsive point source. So, in these specific conditions, the inhomogeneous version of the wave equation can be avoided by suppressing its source term. This was corroborated by numerical results performed in a homogeneous media model.

The use of this initial condition technique has some limitations. It produces wavefronts with a time lag with respect to the ones generated by the IPS's, if we consider the time required for the source operation. Furthermore, it instantly affects all the spatial range covered by the wavelet, while the IPS directly operates only on a point. In non-homogeneous media, where the velocity of wave propagation varies with the position, this can lead to the formation of slightly different waveforms between the two methodologies.

We believe that this study can be expanded to the 2D and 3D cases, what would make it suitable for practical applications such as wave propagation modeling for seismic imaging. However, one has to note that the wavelet that sets up the initial time derivative condition would have the same dimensions as the problem, while the wavelet that sets up the source term would continue to be a one-dimensional function. For this expansion to be made analytically, one would have to deal with the Kirchoff's formula for the solution of the wave equation in  $\mathbb{R}^2$  and  $\mathbb{R}^3$ .

## 7 Acknowledgments

The author wish to dedicate this work to the memory of prof. Liacir dos Santos Lucena, and gratefully acknowledge the support of the Universidade Federal do Rio Grande do Norte (UFRN) and Universidade Federal Rural do Semi-Árido (UFERSA).

## A Obtaining the $S^\psi$ solution

Here, we aim to obtain the  $S^\psi$  solution when one uses an Impulsive Point Source (IPS) as described by the definition (8). From the expression (9), since  $\psi(t' - t_0)$  does not depend on  $x'$ :

$$S_{c,x_s,t_s}^\psi(x,t) = \frac{1}{2c} \int_0^t \psi(t' - t_s) \int_{x-c(t-t')}^{x+c(t-t')} \delta(x' - x_s) dx' dt'$$

Let us make the transformation  $r = c(t - t')$ , so that  $t' = (r + ct)/c = r/c + t$ ,  $dt' = -dr/c$ , and the interval of integration  $0 \rightarrow t$  becomes  $ct \rightarrow 0$ :

$$S_{c,x_s,t_s}^\psi(x,t) = -\frac{1}{2c^2} \int_{ct}^0 \psi(r/c + t - t_s) \int_{x-r}^{x+r} \delta(x' - x_s) dx' dr$$

Let  $I_{x_s}(x, r)$  be the result of the integral in  $x'$ , which, taking into account that  $r \geq 0$ , can be defined by the boxcar function:

$$I_{x_s}(x, r) = \int_{x-r}^{x+r} \delta(x' - x_s) dx' = \Pi_{x-r, x+r}(x_s)$$

which, in turn, can be written in terms of the Heaviside Step Function:

$$I_{x_s}(x, r) = H_{x-r}(x_s) - H_{x+r}(x_s)$$

where  $H_a(x) = H(x - a)$ . Rewriting it in function of  $r$ :

$$I_{x_s}(x, r) = H_{x-x_s}(r) - H_{x-x_s}(-r)$$

One can verify that:

$$H_{x-x_s}(r) - H_{x-x_s}(-r) = H_{|x-x_s|}(r) - H_{|x-x_s|}(-r) \quad (47)$$

The non-null values of the last term in (47) are out of the interval  $0 \leq r \leq ct$ , and, therefore, we can consider:

$$I_{x_s}(x, r) = H_{|x-x_s|}(r)$$

which is equivalent to the following condition:

$$I_{x_s}(x, r) = \begin{cases} 1, & \text{if } r > |x - x_s| \\ 1/2 & \text{if } r = |x - x_s| \\ 0, & \text{otherwise} \end{cases} \quad (48)$$

Coming back to the variable  $t'$ :

$$\begin{aligned} I_{x_s}(x, r) &= H_{|x-x_s|}[c(t - t')] \\ &= H\left[c\left(t - t' - \frac{|x - x_s|}{c}\right)\right] \end{aligned}$$

By using the identity  $H(ax) = H(x)H(a) + H(-x)H(-a)$ , we obtain:

$$I_{x_s}(x, r) = H(c)H\left(t - t' - \frac{|x - x_s|}{c}\right) + H(-c)H\left(-t + t' + \frac{|x - x_s|}{c}\right)$$

But, considering that  $c \geq 0$ , we have  $H(c) = 1$  and  $H(-c) = 0$ :

$$\begin{aligned} I(r) &= H\left(t - t' - \frac{|x - x_s|}{c}\right) \\ &= H_{-(t-|x-x_s|/c)}(-t') \end{aligned}$$

Thus, we arrive at:

$$\begin{aligned} S_{c,x_s,t_s}^\psi(x,t) &= -\frac{1}{2c^2} \int_{ct}^0 \psi(r/c + t - t_s) I_{x_s}(x, r) dr \\ &= \frac{1}{2c} \int_0^t \psi(t' - t_s) H_{-(t-|x-x_s|/c)}(-t') dt' \end{aligned}$$

The function  $H_{-a}(-x)$ , for  $a \geq 0$ , is non-null only for  $x \leq a$ , and, therefore, the interval of integration becomes:

$$S_{c,x_s,t_s}^\psi(x,t) = \frac{1}{2c} \int_0^{t-|x-x_s|/c} \psi(t' - t_s) dt'$$

with  $\varphi(x)$  being the antiderivative of  $\psi(x)$ . By applying the fundamental theorem of calculus, we then get the expression (10).

## B Obtaining the $G^\psi$ solution

From (6):

$$G_{c,x_s}^\psi(x,t) = \frac{1}{2c^2} \int_{x-ct}^{x+ct} \psi\left(\frac{x' - x_s}{c}\right) dx'$$

Let  $\eta = \frac{x' - x_s}{c}$ , so that  $dx' = c d\eta$ :

$$G_{c,x_s}^\psi(x,t) = \frac{1}{2c} \int_{(x-x_s)/c-t}^{(x-x_s)/c+t} \psi(\eta) d\eta$$

Since  $\varphi$  is the antiderivative of  $\psi$ , by the fundamental theorem of calculus we get solution (12):

$$G_{c,x_s}^\psi(x,t) = \frac{1}{2c} \left[ \varphi\left(\frac{x-x_s}{c} + t\right) - \varphi\left(\frac{x-x_s}{c} - t\right) \right]$$

## C Calculus of $\sigma_{\omega_p}$

In this appendix, we derive the standard deviation  $\sigma_{\omega_p}$  of the gaussian function  $f_g$  that corresponds to the antiderivative of  $\varphi_{\omega_p}^r$ . Since both  $f_g$  and  $\varphi_{\omega_p}^r$  have zero mean (no constants are added):

$$f_g(t) = \int \varphi_{\omega_p}^r(t) dt = \int t e^{-\omega_p^2 t^2 / 4} dt = -\frac{2e^{-\omega_p^2 t^2 / 4}}{\omega_p^2}$$

By comparing this with the general form of the gaussian function centered at zero  $ae^{-x^2/2\sigma^2}$ , where  $a$  is an amplitude factor and  $\sigma$  is its standard deviation, we arrive at the conclusion that

$$\sigma_{\omega_p} = \sqrt{2}/\omega_p$$

## D Limit of $E^{S^r}$

We want to prove the (36) relation, corresponding to the maximum value of the total energy of the  $S^r$  solution, which approaches its limit as  $t$  tends to infinity.

By expanding (35), we get

$$E_{c,\omega_p}^{S^r}(t) = \frac{3}{8c\omega_p} \sqrt{\frac{\pi}{2}} \operatorname{erf}\left(\frac{\omega_p t}{\sqrt{2}}\right) + \frac{3}{8c\omega_p} \sqrt{\frac{\pi}{2}} + \frac{te^{-\frac{1}{2}\omega_p^2 t^2}}{8c} - \frac{\omega_p^2 t^3 e^{-\frac{1}{2}\omega_p^2 t^2}}{8c}$$

Since the gaussian function  $e^{-\frac{1}{2}\omega_p^2 t^2}$  is rapidly decreasing, the last two terms tend to zero as  $t \rightarrow \infty$ . The erf function tends to 1, so:

$$\lim_{t \rightarrow \infty} E_{c,\omega_p}^{S^r}(t) = \frac{3}{8c\omega_p} \sqrt{\frac{\pi}{2}} + \frac{3}{8c\omega_p} \sqrt{\frac{\pi}{2}} = \frac{3}{4c\omega_p} \sqrt{\frac{\pi}{2}}$$

validating (36).

## References

- [Habets(2006)] Emanuel AP Habets. Room impulse response generator. *Technische Universiteit Eindhoven, Tech. Rep.*, 2(2.4):1, 2006.
- [Allen and Berkley(1979)] Jont B Allen and David A Berkley. Image method for efficiently simulating small-room acoustics. *The Journal of the Acoustical Society of America*, 65(4):943–950, 1979.
- [Ward and Abhayapala(2001)] Darren B Ward and Thushara D Abhayapala. Reproduction of a plane-wave sound field using an array of loudspeakers. *IEEE Transactions on speech and audio processing*, 9(6):697–707, 2001.

- [Tiwana et al.(2017)Tiwana, Ahmed, Mann, and Naqvi] MH Tiwana, Shakeel Ahmed, AB Mann, and QA Naqvi. Point source diffraction from a semi-infinite perfect electromagnetic conductor half plane. *Optik-International Journal for Light and Electron Optics*, 135:1–7, 2017.
- [Vlaar(1966)] NJ Vlaar. The field from an sh point source in a continuously layered inhomogeneous half-space ii. the field in a half-space. *Bulletin of the Seismological Society of America*, 56(6):1305–1315, 1966.
- [Vidale and Helmberger(1988)] John E Vidale and Donald V Helmberger. Elastic finite-difference modeling of the 1971 san fernando, california earthquake. *Bulletin of the Seismological Society of America*, 78(1):122–141, 1988.
- [Frankel(1993)] Arthur Frankel. Three-dimensional simulations of ground motions in the san bernardino valley, california, for hypothetical earthquakes on the san andreas fault. *Bulletin of the Seismological Society of America*, 83(4):1020–1041, 1993.
- [Evans(1997)] Brian J Evans. *A handbook for seismic data acquisition in exploration*. Society of exploration geophysicists, 1997.
- [Meunier(2011)] Julien Meunier. *Seismic acquisition from yesterday to tomorrow*. Society of Exploration Geophysicists, 2011.
- [Baysal et al.(1983)Baysal, Kosloff, and Sherwood] Edip Baysal, Dan D Kosloff, and John WC Sherwood. Reverse time migration. *Geophysics*, 48(11):1514–1524, 1983.
- [McMechan(1989)] George A McMechan. A review of seismic acoustic imaging by reverse-time migration. *International Journal of Imaging Systems and Technology*, 1(1):18–21, 1989.
- [Virieux and Operto(2009)] Jean Virieux and Stéphane Operto. An overview of full-waveform inversion in exploration geophysics. *Geophysics*, 74(6):WCC1–WCC26, 2009.
- [Cohen and Bleistein(1979)] Jack K Cohen and Norman Bleistein. Velocity inversion procedure for acoustic waves. *Geophysics*, 44(6):1077–1087, 1979.
- [Alford et al.(1974)Alford, Kelly, and Boore] RM Alford, KR Kelly, and D Mt Boore. Accuracy of finite-difference modeling of the acoustic wave equation. *Geophysics*, 39(6):834–842, 1974.
- [D’Alembert(1747)] Jean le Rond D’Alembert. Recherches sur la courbe que forme une corde tendue mise en vibration: Suite. *Histoire de l’Académie Royale des Sciences et des Belles Lettres de Berlin*, page 220, 1747.
- [Miersemann(2012)] Erich Miersemann. *Partial Differential Equations Lecture Notes*. Citeseer, 2012.
- [Drábek and Holubová(2014)] Pavel Drábek and Gabriela Holubová. *Elements of partial differential equations*. Walter de Gruyter GmbH & Co KG, 2014. pp. 73.
- [Mallat(1999)] Stéphane Mallat. *A wavelet tour of signal processing*. Academic press, 1999.
- [Gholamy and Kreinovich(2014)] Afshin Gholamy and Vladik Kreinovich. Why ricker wavelets are successful in processing seismic data: Towards a theoretical explanation. In *2014 IEEE Symposium on Computational Intelligence for Engineering Solutions (CIES)*, pages 11–16. IEEE, 2014.
- [Wang(2015a)] Yanghua Wang. Generalized seismic wavelets. *Geophysical Journal International*, 203(2):1172–1178, 2015a.
- [Wang(2015b)] Yanghua Wang. Frequencies of the ricker wavelet. *Geophysics*, 80(2):A31–A37, 2015b.
- [Wang(2015c)] Yanghua Wang. The ricker wavelet and the lambert w function. *Geophysical Journal International*, 200(1):111–115, 2015c.
- [Duffin(1970)] Richard James Duffin. Equipartition of energy in wave motion. *Journal of Mathematical Analysis and Applications*, 32(2):386–391, 1970.
- [Kukudzhanov(2013)] Vladimir N Kukudzhanov. *Numerical continuum mechanics*, volume 15. Walter de Gruyter, 2013.
- [Courant et al.(1967)Courant, Friedrichs, and Lewy] Richard Courant, Kurt Friedrichs, and Hans Lewy. On the partial difference equations of mathematical physics. *IBM journal*, 11(2):215–234, 1967.